Journal of Non-Newtonian Fluid Mechanics, 52 (1994) 163–176
Elsevier Science B.V.

Shear and elongational flow properties of fluid S1 from rotational, capillary, and opposed jet rheometry

N. Willenbacher * and R. Hingmann
BASF AG, Polymer Research Division, ZKM/R, Ludwigshafen/Rhein, F.R.G.

(Received September 14, 1993; in final form December 20, 1993)

Abstract

Non-linear shear and elongational flow properties of the ternary fluid S1 have been compared to those of a binary solution with similar linear viscoelastic properties. In contrast to the binary solution, fluid S1 exhibits a flow instability. The onset of this instability in rotational flow is characterized by a critical Deborah number $De_c = 13.5$. Secondary flow causes an irreversible decrease of zero-shear viscosity. A flow-induced degradation of the dissolved polymer has been proved by different analytical methods. However, this effect is not sufficient to account for the observed reduction of η_0, and it is speculated that the irregular flow additionally gives rise to a phase separation or demixing of the originally homogeneous solution. Up to now there is no direct experimental evidence for this hypothesis. Elongational flow properties have been characterized by means of an opposing jet apparatus. Apparent elongational viscosity of fluid S1 increases strongly with increasing apparent elongation rate $\dot{\epsilon}$ and total strain ϵ. A strain-independent equilibrium value is not reached. In the case of the binary solution η_E is independent of $\dot{\epsilon}$ and increases only slightly with increasing ϵ. Strong fluctuations of the force signal are observed in the case of fluid S1 when a critical flow rate is exceeded, indicating secondary flow phenomena.

Keywords: elongational flow; opposed jet rheometry; polymer solutions; rotational flow; S1

1. Introduction

The round robin programme on fluid S1 is part of a European Community Science Project for extensional rheometry on polymer solutions. Although this project is directed at the elongational flow properties of polymer

* Corresponding author.

SSDI 0377-0257(94)01224-0

solutions, a thorough characterization of shear flow including viscoelastic behaviour is necessary both as an input for theoretical considerations, and as a reference for extensional viscosity measurements.

In this contribution we compare shear and elongational flow properties of the ternary fluid S1 with those of a binary solution of polyisobutylene (PIB) in Decalin. Steady and dynamic shear experiments were performed using controlled stress and controlled strain rate rotational rheometers as well as a capillary viscometer. Special emphasis was laid on the characterization of secondary flow phenomena occurring in rotational flow of fluid S1. Elongational flow properties were investigated using a home-made opposing jet rheometer.

2. Experimental

2.1 Instruments

2.1.1 Steady and oscillatory shear

Steady shear viscosity data were obtained with a Carri-Med CS 100 constant stress rotational rheometer using plate and plate geometry (radius $R = 2$ cm; gap width $H = 0.2-1.5$ mm) and a home-made, piston-driven capillary viscometer. This instrument was equipped with a circular die of radius 0.31 mm and length 150 mm. Entrance pressure loss effects were neglected. Oscillatory shear tests were performed on a Carri-Med CS 100 controlled stress instrument too, and in addition on a Rheometrics RFS 8400 controlled strain instrument, both equipped with cone-plate geometry ($R = 3$ cm, cone-angle $\alpha = 2°$ and $R = 2.5$ cm, $\alpha = 2.3°$, respectively.) A frequency range from 0.001 to 100 rad s^{-1} was covered.

2.2.1 Elongational flow

The home-made opposing jet rheometer described in Ref. 1 was used. A schematic representation of the instrument is given in Fig. 1. The flow rate is controlled by application of vacuum. The apparatus is equipped with a force transducer (Hottinger Baldwin Messtechnik, Germany) combined with an elastic tube in order to detect the force acting on a nozzle. According to Ref. 2 the apparent strain rate $\dot{\epsilon}$ is calculated from the volumetric flow rate Q by

$$\dot{\epsilon} = Q/(Ad), \tag{1}$$

where A is the area of the nozzle opening and d is the width of the gap separating the nozzles. The apparent elongational viscosity η_E is related to the force F acting on the nozzle by

$$\eta_E = Fd/Q. \tag{2}$$

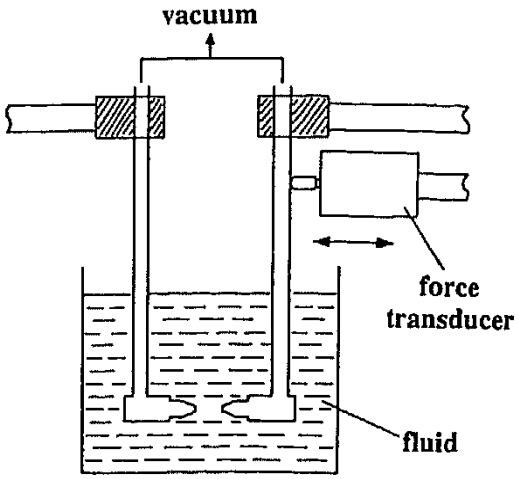

Fig. 1. Schematic representation of the opposing jet rheometer.

An improved analysis of opposing jet data has to take into account the real flow and stress fields, which in turn depend on the rheology of the fluid under consideration and on the geometrical details of the whole configuration. For a Newtonian liquid corresponding calculations have been done by Schunk et al. [3]. An extension of such considerations to viscoelastic fluids has not been tried here.

Two sets of experiments were performed with nozzles of diameter 0.5 mm and 1 mm, respectively. In each set the gap width was varied between 0.5 and 4 mm.

2.2 Samples

The standard fluid S1 was used as delivered. The composition is 2.5% PIB Vistanex L140; 50% polybutene oil (PBO) and 47.5% Decalin.

A binary solution of 5 wt.% PIB in Decalin was prepared according to the specification given in the circular of Professor Ferguson [4] again using Vistanex L140 as PIB component. In the following sections this sample will be referred to as solution A.

In order to avoid cavitation in opposing jet experiments, dispersed air, probably introduced by the stirring process during the preparation of the solutions, had to be removed carefully. To this end, each sample was degassed for 20 h at a pressure of 10^{-6} Pa at room temperature. The loss of Decalin due to this procedure is negligibly small.

Molecular weight and molecular weight distribution of the polymeric component have been determined using different analytical techniques and the results are summarized in Table 1.

The average molecular weight M_v was calculated from the limiting viscosity number $[\eta]$ according to the Mark–Houwink relation

$$[\eta] = KM_v^a, \tag{3}$$

TABLE 1
Molecular weight characterization of fluid S1

Material	Viscometry		SALS	GPC		
	$[\eta]$ ($cm^{-3}\,g^{-1}$)	M_v ($10^6\,g\,mol^{-1}$)	M_w ($10^6\,g\,mol^{-1}$)	M_n ($10^6\,g\,mol^{-1}$)	M_w ($10^6\,g\,mol^{-1}$)	M_w/M_n
Fluid S1 untreated	673	2.56	2.38	0.36	1.70	4.7
Fluid S1 sheared	657	2.47	2.15	0.41	1.59	3.9
Vistanex L140	572	2.03	2.31	0.53	2.67	5.0

with $K = 22 \times 10^{-3}\,cm^3\,g^{-1}$ and $a = 0.7$ [5], since Decalin was used as solvent.

The weight average molecular weight M_w was derived from small angle light scattering experiments (SALS). *n*-Heptane was used as solvent in this case, thus achieving a scattering intensity one order of magnitude higher than in the system PIB–Decalin. Molecular weight distribution was deduced from gel permeation chromatography (GPC) performed on an instrument (Millipore Waters 150 C) calibrated by a set of eight narrow-distributed PIB standards (Polymer Standard Service, Germany). Samples were dissolved in 1,2,4-trichlorobenzene.

3. Results and discussion

3.1 Steady and oscillatory shear flow

Shear viscosity functions for the solutions S1 and A measured in steady as well as oscillatory mode are shown in Fig. 2. In both cases oscillatory shear data from different instruments agree very well. For solution A the results from rotational steady shear are in good agreement with those from capillary viscometry. Moreover the Cox–Merz rule [6], $|\eta^*|(\omega) = \eta(\dot{\gamma})$, if $\omega = \dot{\gamma}$, holds throughout the whole shear rate/frequency range. In the case of solution S1 deviations from this rule are observed for ω, $\dot{\gamma} > 10\,s^{-1}$. Furthermore the data from rotational steady shear experiments do not fit with the results from capillary viscometry for $\dot{\gamma} > 500\,s^{-1}$ and in both cases an apparent "shear-thickening" behaviour is observed, if a critical shear rate $\dot{\gamma}_c$ is exceeded. This is attributed to the occurrence of a flow instability. Similar phenomena are well known for polymeric liquids and have been reviewed recently [7]. A detailed discussion of the flow instability occurring in fluid S1 is given in Section 3.2.

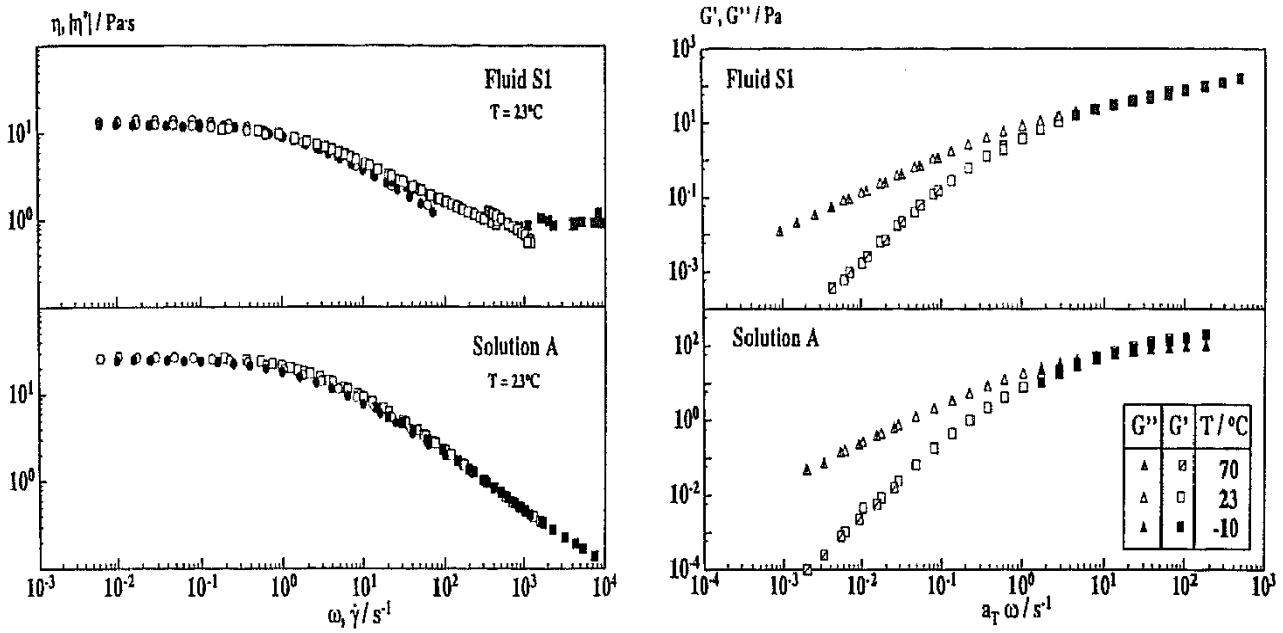

Fig. 2. Viscosity functions of fluids S1 and solution A: ○, oscillatory shear, Carri-Med CS 100; ●, oscillatory shear, Rheometrics RFS 8400; □, steady shear, Carri-Med CS 100; ■, steady shear, KVM, $L/R = 484$.

Fig. 3. Master curve of the dynamic moduli G', G'' of fluid S1 and solution A vs. angular frequency ω for $T = 23°C$.

Master curves of the dynamic moduli G' and G'' for the solutions S1 and A are plotted in Fig. 3 as a function of angular frequency. The original data were measured at various temperatures between -10 and 70°C and were subsequently shifted to the reference temperature of 22°C. From the limiting behaviour of G' and G'' at small frequencies the primary normal stress coefficient $\Psi_{1,0} = \lim 2G'/\omega^2$ and $\eta_0 = \lim G''/\omega$ as well as a characteristic retardation time $\tau = \Psi_{1,0}/2\eta_0$ and the steady-state compliance $J_0^e = \tau/\eta_0$ were calculated. The results are listed in Table 2. The temperature dependence of η_0 is of Arrhenius type in the above mentioned temperature range, which is far above T_g ($-132°C$ for solution A, $-99°C$ in the case of fluid S1). The corresponding values of the activation energy E_0 are also given in Table 2.

3.2 Flow instabilities

Flow instabilities, that means deviations from steady laminar flow, were observed in the circular flow field of plate-plate and cone-plate rotational rheometers as well as in capillary flow. This contribution deals with the phenomena occurring in rotational viscometry. All experiments were carried out on a controlled stress rheometer (Carri-Med CS 100). The imposed shear stress was increased linearly up to a peak value depending on the geometry of the fixtures used. The time interval for this stress sweep was chosen to be 15 min and was kept constant throughout all experiments referred to in this section.

TABLE 2

Rheological parameters of solutions S1 and A at $T = 22°C$

Parameter	Symbol	Solution S1	Solution A	Decalin/PBO (48:52)	Decalin
Zero shear rate viscosity	η_0 (Pa.s)	12.0 ± 0.8	25.0 ± 1.3	0.066 ± 0.003	0.0024 ± 0.0001
$\lim_{\omega \to 0} G''/\omega$	η_0 (Pa.s)	12.6 ± 0.7	26.3 ± 1.2		
Primary normal stress coefficient	Ψ_{10} (Pa.s)	31.4 ± 3.2	55.8 ± 5.6		
Steady-state compliance	J_0^e (Pa^{-1})	0.1 ± 0.002	0.04 ± 0.091		
Characteristic retardation time	τ (s)	1.3 ± 0.1	1.1 ± 0.07		
Activation energy	E_0 (kJ mol^{-1})	35.8 ± 5.1	18.1 ± 3.6	30.7 ± 4.7	

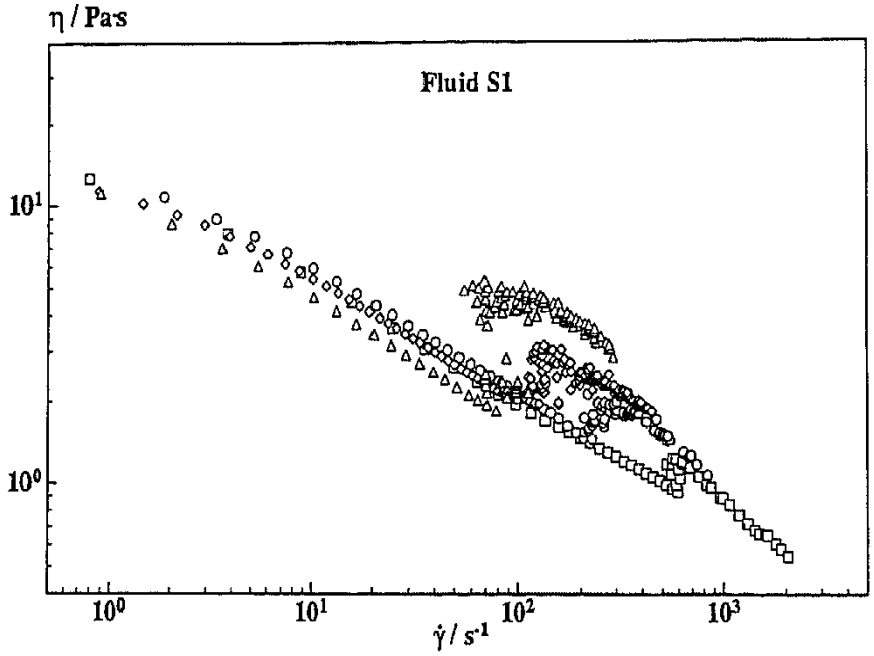

Fig. 4. Apparent "shear-thickening" behaviour of fluid S1 in rotatinal shear flow between parallel plates (radius, 1 cm) with gap height: □, 200 μm; ○, 500 μm; ◇, 1000 μm; △, 1500 μm.

The instability occurring in these experiments can be described as follows. When a critical shear rate $\dot{\gamma}_c$ is reached, an apparent increase in viscosity is observed as shown in Fig. 4. Simultaneously the flow becomes unstable. The surface of the sample starts to fluctuate, loosing its original circular shape. By staining the sample with a red dye and using a glass plate as upper fixture, it could be seen that the material is pulled towards the axis of the

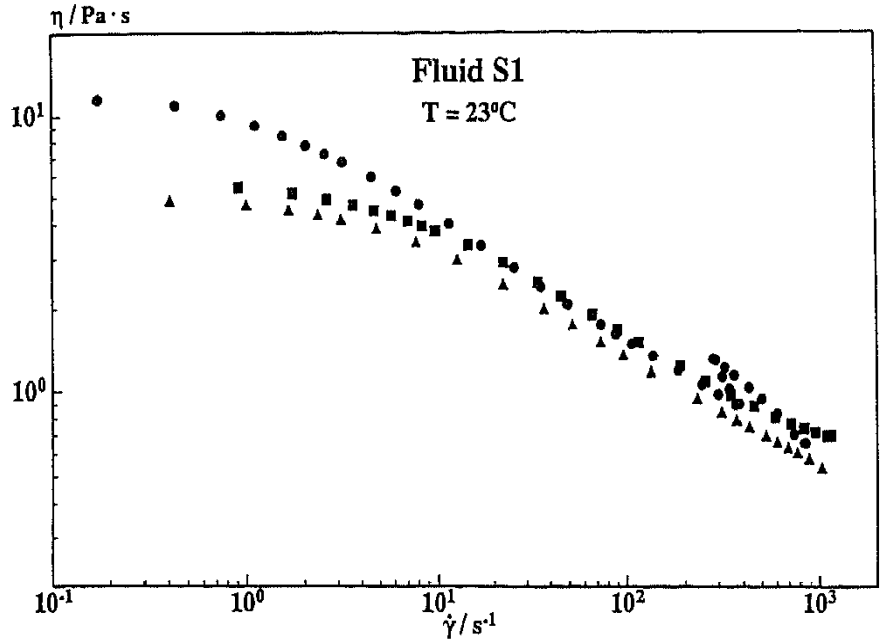

Fig. 5. Viscosity vs. shear rate for fluid S1; subsequent runs on the same sample; Stress-sweep; 0–795 Pa within 15 min. ●, fresh sample; ▲, measurement immediately after first run; ■, measurement 20 days after first run.

rheometer, indicating strong normal forces. This movement towards the rotational axis is irregular. Those observations are very similar to the findings described in Refs. 1, 8 and 9. When an upper critical shear rate $\dot{\gamma}_{cu}$ is reached a stable laminar flow turns up again and the sample spreads out homogeneously over the whole gap. The upper critical shear rate also depends on geometry and is not reached for all geometries, due to the limited angular velocity of the rheometer.

Fluid S1 undergoes an irreversible change when sheared at shear rates higher than $\dot{\gamma}_c$. In a second run with the same material no flow instability is observed and furthermore the zero shear viscosity η_0 decreases by a factor of two (Fig. 5). Even 20 days after initial shearing at $\dot{\gamma} > \dot{\gamma}_c$ the original structure or composition is not recreated and neither flow instability nor a recovery of the original viscosity function is observed in subsequent shear stress sweeps. This effect might be due to a degradation of the polymer molecules induced by the irregular flow field, as has been proposed by several authors [1,9] for fluid M1, which shows a similar instability.

In order to check this hypothesis, untreated samples of fluid S1 as well as samples sheared at shear rates $\dot{\gamma} > \dot{\gamma}_c$ have been analysed with respect to the average molecular weight and molecular weight distribution of the polymeric component as described in Section 2.2 for the pure Vistanex L140 and the results are listed in Table 1, too. PBO and Decalin have not been removed from the solutions for this analysis, although the original samples had to be diluted in different solvents depending on the particular require-

ments of the respective experimental technique. Specific interactions between these solvents and the mixed solvent Decalin–PBO of the primary solutions have not been considered here. A comparison of the results for fluid S1 (untreated) and pure Vistanex L140 shows that such effects can be neglected in SALS experiments. Viscosity measurements on dilutions of fluid S1 yield a limiting viscosity number $[\eta]$, which is significantly higher than that obtained from dilute solutions of the pure Vistanex L140. On the other hand the GPC curves for S1 are shifted towards lower values compared to the results for the pure PIB solution. Both effects can be attributed to an enhancement of the dilute solution viscosity due to the presence of the PBO in fluid S1. Since the PBO component is present in the sheared as well as in the untreated material, these results can be taken as relative values at least. Apart from this restriction the applied analytical techniques show that a degradation of the polymer molecules is induced by the irregular flow at shear rates $>\dot{\gamma}_c$. This can be seen from the decrease of M_v and M_w and from the narrowing of the molecular weight distribution showing up in a decrease of M_w/M_n. Using the SALS result for the reduction of M_w, and assuming $\eta_0 \sim M_w^{3.4}$, a factor of 0.71 is estimated as a lower limit for the decrease of zero shear viscosity. The experimentally observed reduction factor of 0.5 is significantly lower than this estimated value. Therefore it can be concluded that (1) the flow instability gives rise to a degradation of the polymer component of fluid S1– and (2) this degradation is accompanied by another phenomenon resulting in a further flow induced reduction of η_0. Possibly the second process is a kind of demixing or phase separation, but so far there is no experimental evidence for this speculation.

The onset of the flow instability depends on the geometry of the gap. Measurements were carried out using plate-plate fixtures with radii 10 and 20 mm at various gap heights H between 0.2 and 1.5 mm. Temperature was kept constant at $T = 23°C$ in these experiments. In Fig. 6 the critical shear rate is plotted as a function of $1/H$ for both radii. The linear relationship shows that the flow instability starts off at a critical angular velocity $\Omega_c = 11.2 \pm 0.7\ s^{-1}$ independent of plate separation and radius. In addition approximately the same value $\Omega_c = 12.2\ s^{-1}$ was determined using cone-plate geometry ($R = 2cm$; $\alpha = 2°$).

In a second set of experiments the dependence of $\dot{\gamma}_c$ on temperature was determined. Plates with radii 10 and 20 mm were used but the gap height was kept constant at 0.5 mm. Again $\dot{\gamma}_c$ is found to be proportional to the plate radius. In Fig. 7 the product $\eta_0\Omega_c$ is plotted vs. temperature. Obviously this quantity is independent of temperature within the limits of experimental error. The characteristic retardation time τ determined from oscillatory shear experiments (see Section 3.1) varies with temperature in the same manner as η_0. Therefore it seems to be appropriate to characterize the

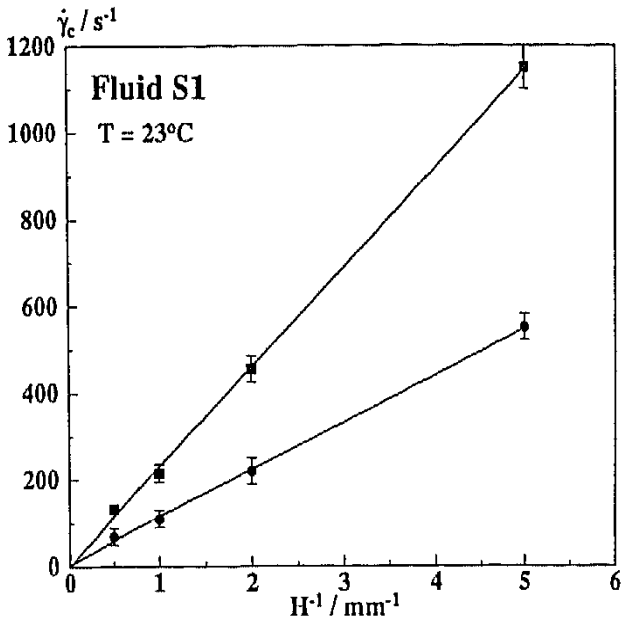

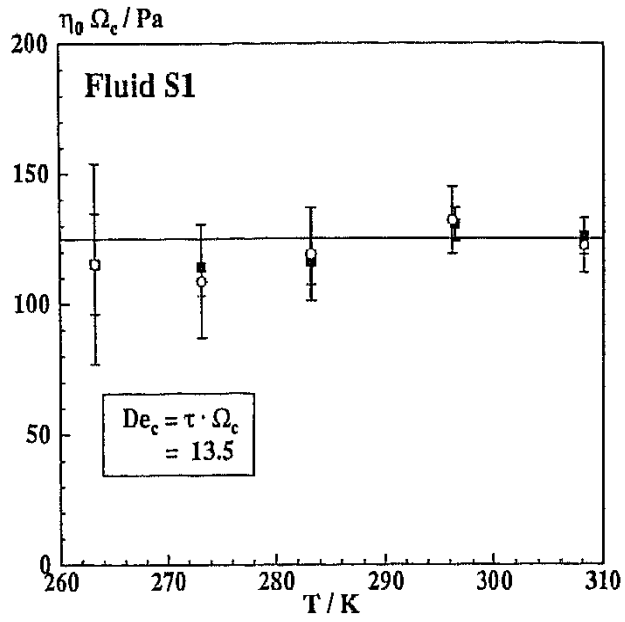

Fig. 6. Critical shear rate $\dot{\gamma}_c$ vs. reciprocal gap height $1/H$; plate-plate geometry; ■, $R = 2$ cm; ●, $R = 1$ cm. The critical angular velocity Ω_c is calculated from the slope of the straight line fitted to the experimental data, according to the equation $\dot{\gamma}_c = \Omega_c R/H$.

Fig. 7. $\eta_0 \Omega_c$ vs. temperature T; plate-plate geometry ($H = 0.5$ mm); ■, $R = 2$ cm; ○, $R = 1$ cm.

onset of the flow instability by a critical Deborah number [10]

$$De_c = \tau \Omega_c. \tag{4}$$

Using the values for the critical angular frequency and the characteristic retardation time as given above, a critical Deborah number $De_c = 13.5 \pm 1.9$ is obtained. This quantity characterizes the onset of the instability occurring in circular flow of fluid S1, independent of temperature and dimensions of the plate-plate and cone-plate fixtures used.

Several authors [8,9] have shown that the onset of flow instabilities occurring in other PIB solutions of similar composition is characterized by critical Deborah numbers, too. In contrast to S1 these fluids showed Boger-type flow behaviour and the values for De_c were in reasonable agreement with theoretical predictions of Phan-Thien derived for an Oldroyd-B fluid [11], although the experimentally observed instabilities were not of the same type as assumed there. The Phan-Thien analysis predicts a critical Deborah number given by

$$De_c = \pi / \sqrt{(1-\beta)(5-2\beta)}, \tag{5}$$

where $\beta = \eta_s/\eta_0$ is the ratio of the solvent viscosity to the total viscosity of the solution. In the case of solutions S1 and A the parameter β is negligibly small and therefore both fluids should exhibit a flow instability at $De_c = 1.4$. Obviously the Phan-Thien criterion can not be applied to these shear-thinning viscoelastic fluids.

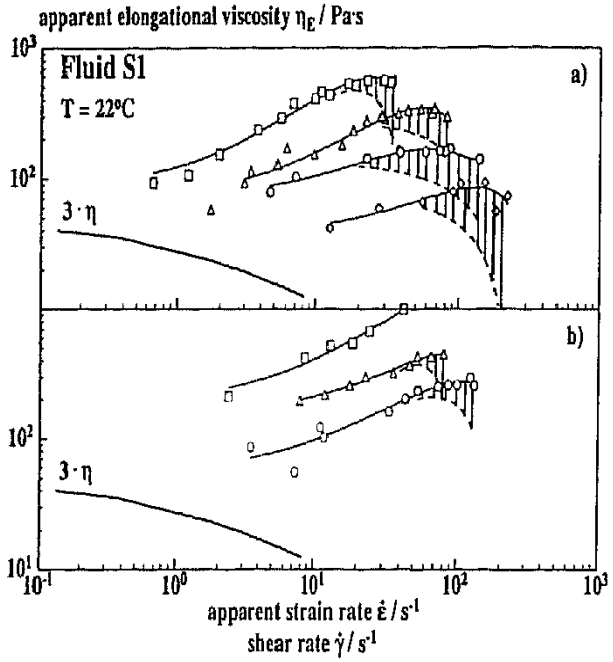

Fig. 8. Apparent elongational viscosity of fluid S1 vs. apparent strain rate as measured by the opposing jet technique; nozzle separations; ◇, 0.5 mm; ○, 1 mm; △, 2 mm; □, 4 mm: (a) nozzle diameter 1 mm; (b) nozzle diameter 0.5 mm. Lines are drawn to guide the eyes; full line, shear viscosity times three. The shaded area indicates the corresponding fluctuations of the force signal in the respective range of apparent strain rates.

3.3 Elongational flow

Elongational flow properties of solutions S1 and A have been characterized by means of an opposing jet rheometer. Each sample had been degassed carefully and the absence of cavitation in our opposing jet experiments was checked visually. To this end, the tubes connecting the nozzles and the vacuum pump were partly made out of glass. Experiments on fluid S1 were performed using nozzles of diameter 0.5 and 1 mm. Gap settings of 0.5, 1, 2 and 4 mm were investigated. The results are presented in Fig. 8. The apparent elongational viscosity η_E is almost independent of the diameter of the nozzles used in these measurements, but rises strongly with increasing gap width. This result suggests a pronounced increase of elongational viscosity with increasing deformation, since the total strain exerted on a fluid element in these experiments is proportional to the product $\dot{\epsilon}d$. But obviously the total deformation is too small to reach a strain-independent plateau value. Similar results have been reported by Schweizer et al. [12] for fluid M1. The shape of the η_E vs. $\dot{\epsilon}$ curves remains approximately the same for all gap settings. At low strain rates η_E starts at a level corresponding to a Trouton ratio η_E/η of about 3 and increases with increasing $\dot{\epsilon}$, passing through a maximum at a characteristic strain rate $\dot{\epsilon}_m$. The similarity of the shape of the curves obtained for different geometrical parameters suggests shifting the data onto a single master curve. In a coarse approximation this can be done by plotting η_E/d

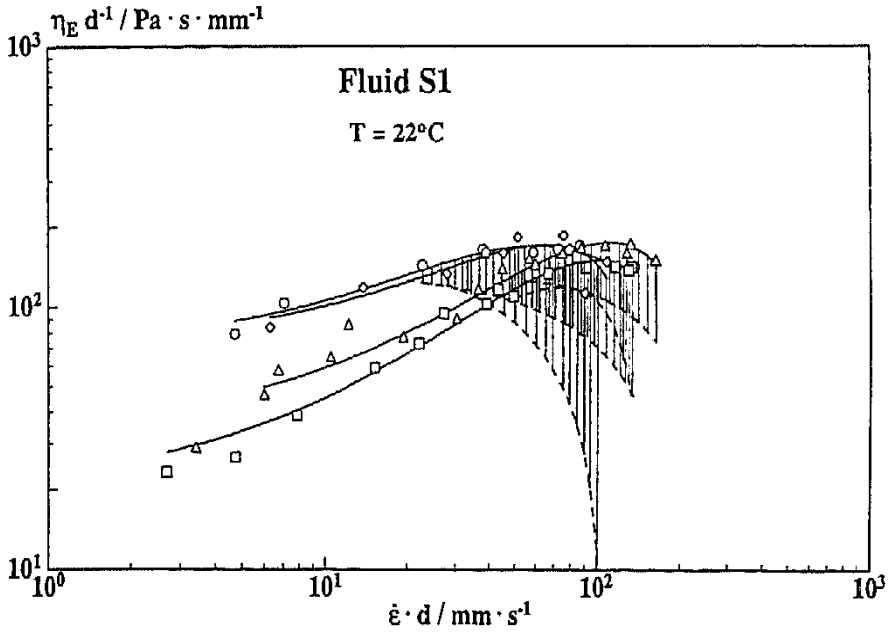

Fig. 9. η_E/d vs. $\dot{\varepsilon}d$ for fluid S1 using the data shown in Fig. 8(a).

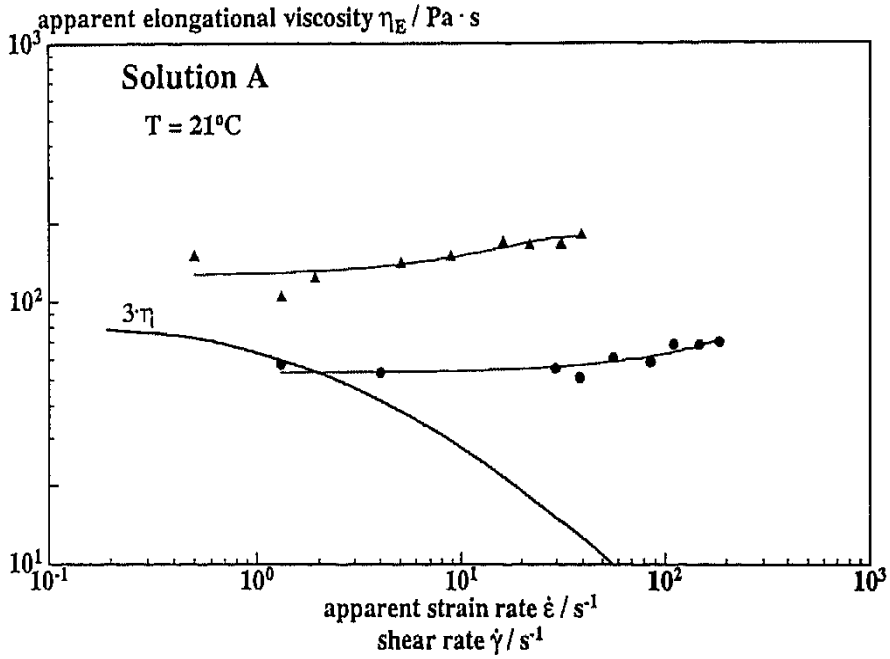

Fig. 10. Apparent elongational viscosity of solution A vs. apparent strain rate as measured by the opposing jet technique (nozzle diameter 1 mm); nozzle separations; ●, 1 mm; ▲, 4 mm. Lines are drawn to guide the eyes; full line, shear viscosity times three.

vs. $\dot{\varepsilon}d$ as is shown in Fig. 9. Especially the maxima of the original curves coincide in this representation, showing that the peak value of η_E occurs at a characteristic level of total strain, independent of geometry.

In the case of solution A measurements were done using nozzles of 1 mm diameter at separations of 1 mm and 4 mm, respectively. The results are shown in Fig. 10. The apparent elongational viscosity η_E is approximately independent of strain rate. Its absolute value increases by a factor of two,

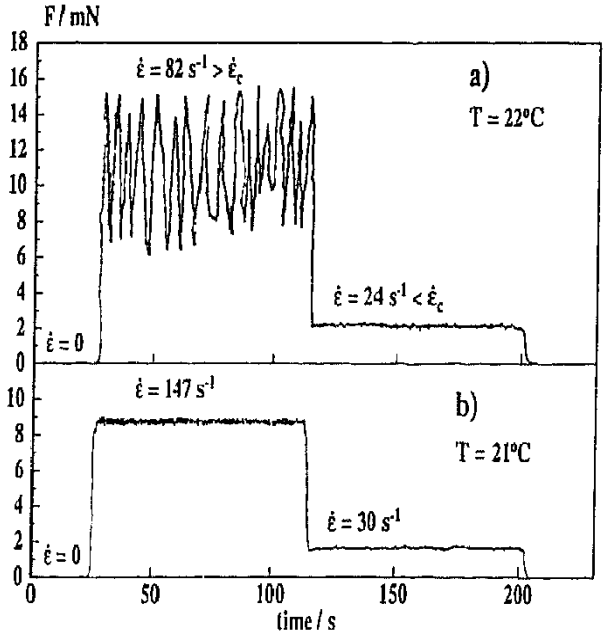

Fig. 11. Force signal measured at the nozzle of the opposing jet rheometer: (a) fluid S1; (b) solution A.

when changing gap width from 1 to 4 mm, and therefore the dependence on total strain is less pronounced than in the case of fluid S1.

The flow of fluid S1 in the opposing jet apparatus is not stable throughout the whole range of strain rates examined. When a critical value $\dot{\epsilon}_c$ is exceeded strong fluctuations of the force signal are observed (Fig. 11), which, in analogy to the findings in shear flow, are attributed to secondary flow phenomena. This secondary flow has not been proved directly here, but our observations are very similar to those reported by Schweizer et al. for fluid M1 [12], and previously by Keller et al. [13] for dilute solutions of high molecular weight polystyrene and polyethylene oxide. These authors have proved the occurrence of flow instabilities in opposing jet type flow fields, using birefringence techniques. Due to the fluctuations of the force signal, the elongational viscosity η_E is no longer well defined. The data shown in Figs. 8 and 9 were calculated from the maxima of the corresponding force signals and fluctuations are indicated by the shaded areas in these Figures. The critical strain rate $\dot{\epsilon}_c$ is somewhat lower than $\dot{\epsilon}_m$ and varies between 8 and 60 s^{-1}, depending on gap width. But the corresponding quantity $\dot{\epsilon}_c d$ is almost independent of the gap setting (Fig. 9). No flow instabilities were observed in the case of solution A.

4. Summary and conclusion

Shear and elongational flow properties of the ternary system S1 have been compared to those of a binary solution of PIB in Decalin (solution A).

Whereas the linear viscoelastic properties of both solutions are very similar, strong differences are observed in non-linear flow. Flow instabilities occur in rotational as well as capillary flow of fluid S1, but not for solution A. The onset of the instability in rotational flow of fluid S1 is characterized by a critical Deborah number $De_c = 13.5$, independent of temperature and dimensions of the plate-plate and cone-plate devices used. This is about one order of magnitude higher than predicted by Phan-Thien's analysis, which moreover predicts a secondary flow for solution A, too. Obviously these theoretical considerations do not apply to this shear-thinning, viscoelastic fluid. The secondary flow cuases an irreversible structural change of the material, showing up in a decrease of η_0 by a factor of two. Different analytical methods have revealed a weak degradation induced by the irregular flow at $De > De_c$, which is not sufficient to account for the strong decrease of viscosity. Therefore an additional mechanism must be present, and it is speculated that the secondary flow gives rise to a kind of phase separation or concentration fluctuation. This hypothesis has not yet been proved experimentally, but such phenomena are well known for multi-component polymeric fluids and have been reviewed recently [14]. Nevertheless, the fact that the instability does occur in the ternary system containing both a good (Decalin) and a poor (PBO) solvent for the PIB, but not in the binary solution, is in favour of our hypothesis. Possibly, optical techniques, such as light scattering and birefringence measurements, can help to answer this open question.

The apparent elongational viscosity η_E of fluid S1 as revealed by the opposing jet technique increases strongly as a function of apparent strain rate and total strain. No strain-independent equilibrium value is reached in our experiments. When a critical strain rate is exceeded, strong fluctuations of the force signal are observed, which are attributed to secondary flow phenomena. No such fluctuations are observed in the case of solution A. Furthermore, η_E is approximately independent of strain rate and increases slightly with total strain in the case of this binary solution.

Acknowledgements

The authors would like to thank several colleagues from the Polymer Research Division of BASF for their contributions to this work: Dr. D. Lilge provided the GPC data and Dr. H. Schuch contributed the SALS results. The attentive performance of rheological experiments by Mr. H. Baumann, Mr. R. Benz, Mr. D. Lingenfelder, Mr. J. Steidel and Mr. P. Sternal is also acknowledged.

References

1 H.M. Laun and R. Hingmann, J. Non-Newtonian Fluid Mech., 35 (1990) 137–157.
2 G.G. Fuller, C.A. Cathey, B.Hubbard and B.E. Zebrowski, J. Rheol., 31 (1987) 235.
3 P.R. Schunk, J.M. de Santos and L.E. Scriven, J. Rheol., 34 (1990) 387–414.
4 J. Ferguson, Circular about the S1 project, 1992.
5 J. Brandrup and E.H. Immergut, Polymer Handbook, 3rd edn., J. Wiley, New York, 1989.
6 W.P. Cox and E.H. Merz, J. Polym. Sci., 28 (1958) 612.
7 R.G. Larson, Rheol. Acta, 31 (1992) 213–263.
8 J.J. Magda and R.G. Larson, J. Non-Newtonian Fluid Mech., 30 (1988) 1–19.
9 G.H. McKinley, J.A. Byars, R.A. Brown and R.C. Armstrong, J. Non-Newtonian Fluid Mech., 40 (1991) 201–223.
10 R.B. Bird, R.C. Armstrong and O. Hassager, Dynamic of Polymeric Liquids, Vol. 1, Fluid Mechanics, J. Wiley, New York, 1987.
11 N. Phan-Thien, J. Non-Newtonian Fluid Mech., 13 (1983) 325.
12 T. Schweizer, K. Mikkelsen, C. Cathey and G. Fuller, J. Non-Newtonian Fluid Mech., 30 (1991) 277–286.
13 A. Keller, A.J. Müller and J.A. Odell, Progr. Colloid Polym. Sci., 75 (1987) 179.
14 R.G. Larson, Rheol. Acta, 31 (1992) 497–520.